Standard Article

International Journal of ENGINE RESEARCH

International J of Engine Research
2024, Vol. 25(3) 513–526

DOI: 10.1177/14680874231196987
journals.sagepub.com/home/jer
Sage

Hydrogen combustion in two-stage high-pressure gas turbine—thermal and flow simulations for performance comparison with fossil fuels

Byungwook Kim[1], Thanh Dam Mai[1], Duy-Tan Vo[2], Hyeon Kyun Lee[1], Yoonhyeong Jeong[1], Sungho Chang[3], Hyoungsoon Lee[1,2] and Jaiyoung Ryu[4]

Abstract

Hydrogen energy forms an attractive solution for reducing greenhouse gas emissions from gas turbine systems. Although hydrogen combustion has been widely studied for combustors, only a few studies have considered the combustion effect downstream of the combustor. This study conducted an integral simulation of the combustion and flow of a GE-E^3 aero-engine under hydrogen fuel and compared its performance with that of representative fossil fuels such as Jet A in an aero-engine and methane in an industrial gas turbine. All simulations were conducted under a constant heat input at the combustor and turbine inlet temperatures. During combustion simulation, the HyChem mechanism was applied to evaluate the composition of the products in an equilibrium model. Specifically, Reynolds-averaged Navier–Stokes steady simulation of a two-stage high-pressure gas turbine was conducted using the calculated boundary condition from the combustion simulation and $k-\omega$ shear stress transport γ turbulence model. The results revealed the high velocity of the hydrogen combustion flue gas owing to its low density under a large pressure difference. Overall, the power output, thermal efficiency, and fuel consumption were improved by hydrogen combustion. The thermal and flow results of the simulation can be used to develop hydrogen gas turbines.

Keywords

Gas turbine, hydrogen combustion, aerodynamic characteristics, gas turbine performance, fuel consumption

Date received: 10 May 2023; accepted: 8 August 2023

Introduction

Greenhouse gas emissions from fossil fuels are one of the primary causes of global warming, which is gradually affecting human life through climate change and natural catastrophes. Currently, nonrenewable sources such as coal, oil, and natural gas account for over 80% of the global energy production.[1] Furthermore, with the continually increasing global population and the growing demand for fossil fuels, the cost of these fuels is expected to increase rapidly. Thus, the development of fossil-fuel alternatives for transportation and industrial applications is essential, considering both the environmental, and economic aspects.

As such, hydrogen is a promising alternative to fossil fuels because of its abundant reserves and zero-carbon emission characteristics.[2] Despite the demerits related to its production, transportation, and storage,[3,4] hydrogen is perceived as a vital energy resource because recent technological advancements have resolved these economic and technological limitations.[5] Based on these predictions, researchers have attempted to apply hydrogen to gas turbines. Although the development of hydrogen gas turbines is currently in its early stages,

[1]Department of Mechanical Engineering, Chung-Ang University, Seoul, Republic of Korea
[2]Department of Intelligent Energy and Industry, Chung-Ang University, Seoul, Republic of Korea
[3]Korea Electric Power Corporation Research Institute, Daejeon, Republic of Korea
[4]School of Mechanical Engineering, Korea University, Seoul, Republic of Korea

Corresponding authors:
Hyoungsoon Lee, Department of Mechanical Engineering, Chung-Ang University, Bldg 310 #427, Dongjak-Gu, Seoul 06974, Republic of Korea.
Email: leeh@cau.ac.kr

Jaiyoung Ryu, School of Mechanical Engineering, Korea University, Innovation Building #411, Anam-Ro 145, Seoul 02841, Republic of Korea.
Email: jryu@korea.ac.kr

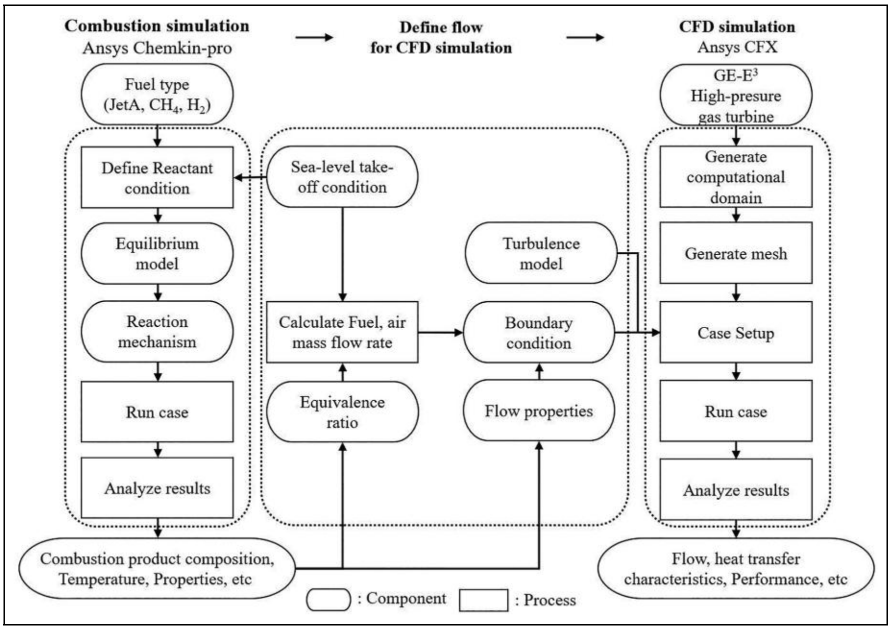

Figure 1. Overall simulation progress for evaluating fuel effects in gas turbines.

significant progress has been achieved in the past decade. Recently, international gas turbine manufacturers have set the goal of developing a 100% hydrogen-operated gas turbine by 2030 and are currently increasing the hydrogen capacity of their gas turbine products.[6,7]

Several studies have been conducted on hydrogen combustion within gas turbine components. Chiesa et al.[8] utilized natural gas mixed with hydrogen gas as a fuel for gas turbines and reported an increase in the combined power output, which eventually reduced the compressor airflow. Cappelletti et al.[9] performed experimental and numerical simulations to assess the impact of a lean premixed burner fueled with pure hydrogen on the performance of gas turbines. Their findings indicated a higher outlet velocity of 80–130 m/s at the combustor outlet with a range of 5–17 ppm at 15% oxygen and an equivalence ratio of 0.25–0.34. These studies analyzed the effects of variations in the combustion environment on gas-turbine combustors. However, most existing research focuses on the combustor only, and only a handful of studies have evaluated the downstream effects of hydrogen combustion in gas turbine combustors.

In addition, several studies employed computational fluid dynamics (CFD) to evaluate the internal characteristics and performance of gas turbines in various applications. Mai and Ryu[10,11] estimated the aerodynamics and heat-transfer effects of a damaged blade in a 1.5-stage high-pressure gas turbine. Nguyen et al.[12] conducted a single-stage high-pressure gas turbine simulation to compare the effects of chemical reactions on the flow parameters. Although numerous studies have explored the characteristics of gas turbines, most of them assume air as the working fluid. The actual composition of the combustion products is crucial for understanding the internal characteristics of actual gas turbines. Therefore, the simulation of an entire gas turbine considering the combustion product as the working fluid is essential.

Thus, simulation of hydrogen applied gas turbine using combustion product as working fluid is required to precisely compare the internal characteristics and performance with current gas turbine systems operating with fossil fuels. This study analyzed the effects of hydrogen combustion on the internal flow, heat transfer characteristics, and performance of the high-pressure gas turbine of an aero engine through combustion and flow simulations in comparison with representative fossil fuels such as Jet A in an aero engine and methane in an industrial gas turbine. The methodology and results of the simulation provide guideline for the future development of hydrogen gas turbine.

Numerical method

Overall process and case classification

This study proposes a simulation process to investigate the impact of various fuels, including hydrogen, on gas turbine performance (Figure 1). In this regard, the GE-E^3 is a dual-spool turbofan aeroengine that has been utilized as a computational model for both combustion and CFD simulations. A schematic of the dual-spool turbofan aeroengine is illustrated in Figure 2. Specifically, to predict the temperature and composition of the combustion products, an equilibrium model was used in the combustion simulation, which computed the expected composition of the combustion output under specific combustion conditions using a chemical reaction mechanism. Thereafter, the boundary conditions for the flow simulation were derived

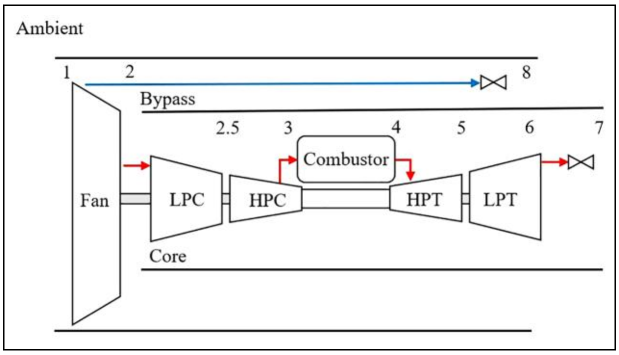

Figure 2. Schematic of dual-spool turbofan aeroengine.

Table 1. Case classification for simulation.

Case ID	Fuel	Chemical formula	Molecular weight (g/mol)	LHV (MJ/kg)
JetA (Reference)	JetA	$C_{11.4}H_{21.7}$	158.6	43.12
CH4	Methane	CH_4	16.04	50
H2	Hydrogen	H_2	2.016	120

from the combustion simulation results and the flow rates specified in the report. A computational domain was generated to conduct a gas turbine flow simulation, and the results were used to analyze the characteristics, and performance of the gas turbine.

The simulation cases used to comparatively analyze the effects of hydrogen combustion and those of the current fuels, JetA and CH_4 (Methane), representing the aero gas turbine fuel and industrial gas turbine fuel, respectively, along with the fundamental chemical properties of the fuels are listed in Table 1. JetA, also referred to as A2 fuel,[13] is a general distillate jet fuel for aeroengines with an average molecular formula of $C_{11.4}H_{21.7}$, comprising 20% *n*-paraffin, 29.4% iso-paraffin, 31.9% cycloparaffin, and 18.7% aromatics.[14] In particular, the lower heating values (LHVs) of the JetA, CH4, and H2 cases were 43.12, 50, and 120 MJ/kg, respectively.

Methods for combustion simulation

As the results vary with the constraints and conditions of the simulation, determining reasonable constraints is vital for conducting the simulation between multiple fuels. As reported in previous studies, a constant heat input is a common constraint for evaluating various fuel compositions in gas turbine combustors.[15,16] Accordingly, in this study, the simulation cases were conducted assuming constant heat input in the combustor, gas turbine inlet pressure, and temperature, similar to the reference case.

The combustion simulations were performed to evaluate the concentrations of the combustion products at the combustor outlet. To evaluate this composition, a chemical equilibrium model was used in the commercial

Table 2. Sea-level takeoff conditions for GE-E^3 combustor.

Parameter	Value
P_3	3.03 MPa
T_3	815 K
$\dot{m}_{total}$	55.3 kg/s
$\dot{m}_f/\dot{m}_a$	0.024
Φ	0.349

program ANSYS ChemkinPro. In the chemical equilibrium model analysis, the equilibrium condition was determined by minimizing Gibb's free energy.[17]

In principle, the kinetic reaction mechanism is a group of reaction equations used for calculating the fractions of the combustion products. In various applications involving the kinetic reaction mechanism, it varies with the number of reaction equations, reaction rate, and other factors. Herein, the HyChem model[18,19] was employed in all cases. A baseline standard-day sea-level take-off condition was applied for the combustion simulation of each fuel in the GE-E^3 combustor.[20] The flow parameters for the combustor of the GE-E^3 aero-engine under sea-level takeoff conditions are listed in Table 2. To perform an ideal premixed combustion simulation of aeroengine under sea-level takeoff condition, the fuel–air mixture was assumed to experience complete combustion under constant pressure and enthalpy conditions, with a pressure of 3.03 MPa and a temperature of 815 K.

Combustion simulation results and boundary condition calculation

The major gas compositions of the combustion products of each fuel are depicted in Figure 3. As observed from Figure 3(a), the H_2O mass fraction increased in the following order: Jet A, CH4, and H2, whereas the CO_2 mass fraction decreased in the same order. The mass fraction of CO_2 in the H2 case was not plotted in Figure 3(a) because CO_2 was excluded from the hydrogen combustion process. Compared to the reference case, the mass fraction of O_2 decreased in the CH4 case, whereas it increased in the H2 case. As portrayed in Figure 3(b), the N_2 mass fraction increased in both the CH4 and H2 cases compared to the JetA case. As the nitrogen mass fraction increased in the CH4 and H2 combustion products, the formation of nitrogen oxide increased concomitantly. The equilibrium temperature of each fuel with respect to the equivalence ratio is displayed in Figure 4, wherein the combustion temperature was sequentially higher for H2, JetA, and CH4 at the same equivalence ratio. Thus, at a certain temperature, hydrogen combustion exhibits a lower equivalence ratio compared to the other fuels.

According to the equivalence ratios listed in Table 2 and the relationship between the equivalence ratio and temperature (Figure 4), the combustion temperature of

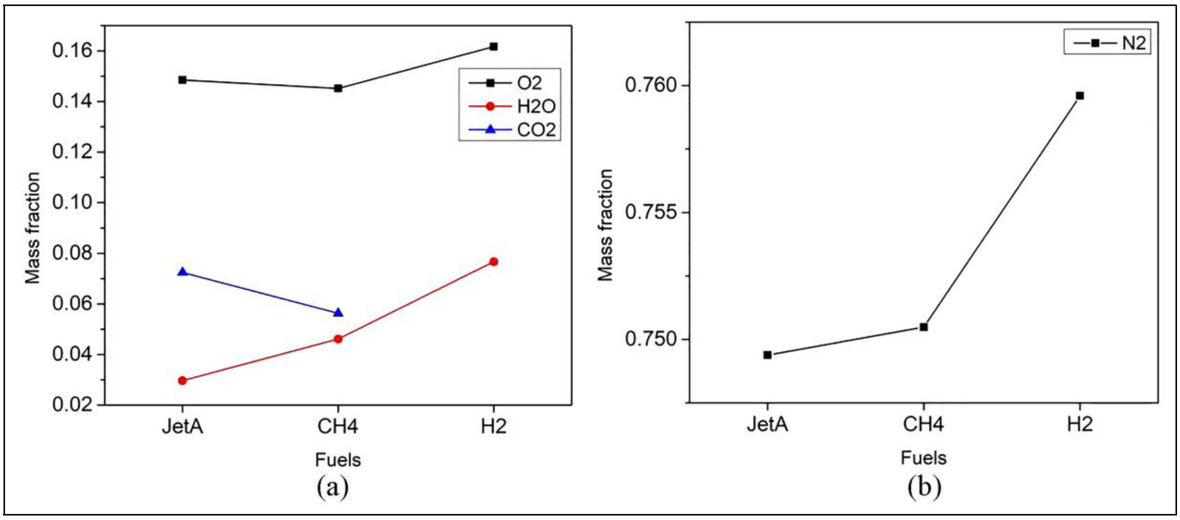

Figure 3. Mass fractions of major combustion products of various fuels: (a) CO_2, H_2O, O_2, and (b) N_2.
CO_2: carbon dioxide; H_2O: water vapor; O_2: oxygen gas; N2: nitrogen gas

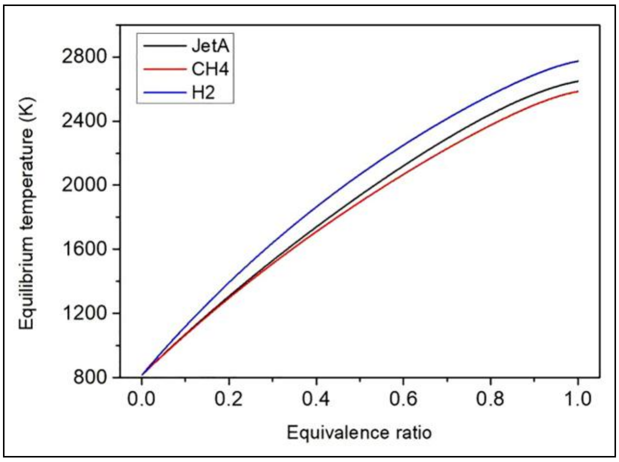

Figure 4. Equilibrium temperature with respect to equivalence ratio.

JetA was estimated to be 1629 K. Based on the assumption related to the fuels (equation (1)) and the definition of their equivalence ratio (equation (2)), the mass flow rate of the fuel and air required for attaining such a temperature can be evaluated for the CFD simulation of each fuel.

$$\dot{m}_f LHV_f = \dot{Q} = Const. \tag{1}$$

$$\Phi = \frac{\left(\frac{\dot{m}_a}{\dot{m}_f}\right)_{stoic}}{\left(\frac{\dot{m}_a}{\dot{m}_f}\right)} \tag{2}$$

$\dot{m}_f$ denotes the fuel mass flow rate, $\dot{m}_a$ indicates the air mass flow rate, LHV_f represents the lower heat value of the fuel, $\dot{Q}$ denotes the heat input rate in the combustor, Φ indicates the equivalence ratio, and $\left(\frac{\dot{m}_a}{\dot{m}_f}\right)_{stoic}$ denotes the theoretical air–fuel ratio of the fuel.

Table 3. Mass flow rate calculation for entire gas turbine under constant heat input from combustor and turbine inlet temperature between cases.

Parameter	JetA	CH4	H2
Φ	0.349	0.359	0.295
$\dot{m}_f$ (kg/s)	1.2961	1.1178	0.4657
$\dot{m}_a$ (kg/s)	54.0039	53.4279	54.1825
$\dot{m}_{total}$ (kg/s)	55.3	54.5456	54.6482

The equivalence ratio for a combustion temperature of 1629 K, fuel and air mass flow rate, and total mass flow rate for various fuels are summarized in Table 3. The equivalence ratio decreased in the order of CH4, JetA, and H2. Under the same heat input in the combustor, H2 exhibited the lowest mass flow rate, whereas the mass flow rates of Jet A and CH_4 fuels were approximately 2.78 and 2.4 times higher than that of hydrogen, respectively. Compared to the JetA case, the mass flow rate of air in the H2 case increased by 0.33%, whereas in the CH4 case, the mass flow rate decreased by 1.06%. Under this assumption, the total mass flow rates of CH4 and H2 decreased by 1.36% and 1.17%, respectively. Owing to the periodic conditions in the gas-turbine CFD simulations, the total mass flow was divided by a factor of 38. The total pressure and temperature at the turbine inlet can be calculated using the flow properties and mass flow rate of the flow information.

Computational domain

As depicted in Figures 5 and 6, the GE-E^3 high-pressure gas turbine model served as the computational domain in the CFD simulations. The first two stages of the model originally comprised 46 stators and 76 rotors in the first stage, and 48 stators, and 70 rotors in the

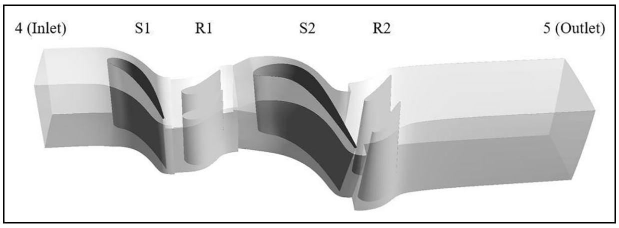

Figure 5. Computational domain for gas turbine simulation.

Figure 6. Overall geometry of GE-E^3 two-stage high-pressure gas turbine.

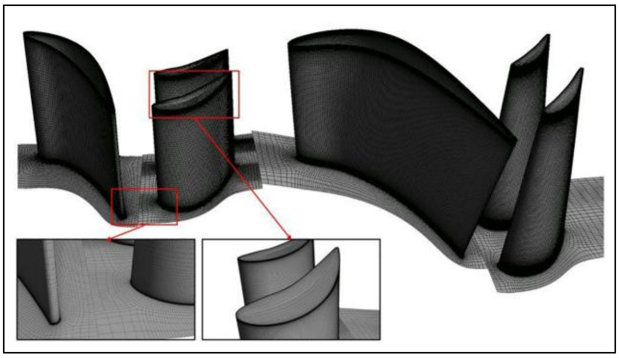

Figure 7. Hexahedra GE-E^3 two-stage high pressure gas turbine.

second stage.[21] To minimize the numerical errors in gas turbine flow simulations, the ratio of stator vanes to rotor blades should be equal to small integers (1/1, 1/2, 2/3, 3/4, etc.). Therefore, the domain-scaling method[22] was employed to adjust the number of blades and vanes without modifying the airfoil shape according to the chord length of the first stator. Consequently, the number of stator vanes and rotor blades selected herein was 38 and 76, respectively. The detailed mesh of the computational domain comprising an unstructured hexahedral mesh type with 11,208,866 nodes is displayed in Figure 7. The number of nodes was maintained similar to that in the previous study and accuracy was ensured by considering a $y+$ value below 0.5 at the blade surface and 1 for the walls. The grid-independence test for the mesh has been performed in a previous study.[23]

Governing equation and numerical method for gas turbine flow simulations

In particular, three governing equations—the continuity, momentum, and energy equations—were used to analyze the fluid flow for steady and compressible flow in a three-dimensional gas turbine. The equations are stated as follows:

$$\frac{\partial \rho}{\partial t} + \frac{\partial}{\partial x_i}(\rho u_i) = 0, \tag{3}$$

$$\frac{\partial}{\partial t}(\rho u_i) + \frac{\partial(\rho u_i u_j)}{\partial x_i} = \frac{\partial P}{\partial x_i} + \frac{\partial}{\partial x_j}\left[\mu\left(\frac{\partial u_i}{\partial x_j} + \frac{\partial u_j}{\partial x_i} - \frac{2}{3}\delta_{ij}\frac{\partial u_k}{\partial x_k}\right)\right] + \frac{\partial\left(\rho\left\{u_i' u_j'\right\}\right)}{\partial x_j}, \tag{4}$$

$$\frac{\partial}{\partial t}(\rho E) + \frac{\partial}{\partial x_j}\left(u_j(\rho E + P)\right) = \frac{\partial}{\partial x_j}\left[(k_{eff})\frac{\partial T}{\partial x_j}\right] + \frac{\partial}{\partial x_j}\left[u_i \mu_{eff}\left(\frac{\partial u_i}{\partial x_j} + \frac{\partial u_j}{\partial x_i} - \frac{2}{3}\delta_{ij}\frac{\partial u_k}{\partial x_k}\right)\right], \tag{5}$$

$i,\ j,\ k = 1, 2, 3$

In equation (3), ρ denotes density and u indicates velocity. In Equation 4, P denotes pressure, μ indicates dynamic viscosity. In equation (5), E symbolizes the specific internal energy, k_{eff} denotes the effective thermal conductivity, and μ_{eff} indicates the effective dynamic viscosity. The commercial software ANSYS CFX was used to solve the governing equations for the gas turbine region.

The selection of a method for the turbulence model is essential to obtain reliable CFD simulation results at an appropriate cost. As such, direct numerical simulation (DNS), large-eddy simulations (LES), and Reynolds-averaged Navier–Stokes (RANS) models are the common turbulence models used in CFD simulations. Although DNS and LES provide a detailed structure of the turbulence, they typically incur a high computational cost.[24–26] In contrast, RANS involves low computational cost with overall reliable results in the turbomachinery.[27–29] Moreover, Choi and Ryu compared various turbulence models under the RANS turbulence model for high-pressure turbulent flows in a three-dimensional gas turbine.[23] They confirmed that the simulation results corresponded well with the experimental data[30] in $k-\omega$ shear stress transport (SST) γ-turbulence model. Therefore, we employed the RANS simulation with $k-\omega$ SST γ-turbulence model to predict the flow and performance of the gas turbine.

Table 4. Boundary and operating conditions.

Location	Parameter	JetA	CH4	H2
Inlet	Total pressure (MPa)	3.0324	3.03243	3.03260
	Total temperature (K)	1631.63	1631.61	1631.69
Outlet	Mass flow rate (kg/s)	1.4452	1.4354	1.4381
R1, R2	Rotor speed (RPM)	13,410.76	13,410.76	13,410.76
Wall	Heat transfer for Adiabatic simulation	Adiabatic	Adiabatic	Adiabatic
	Blade heat transfer for Isothermal simulation (K)	1142	1142	1142

Table 5. Working fluid properties.

		JetA	CH4	H2
Mass fraction	CO_2	0.0728	0.056321	–
	H_2O	0.0298	0.046087	0.076674
	O_2	0.147088	0.145228	0.161725
	N_2	0.748417	0.750483	0.758599
	NO	0.00182	0.001792	0.001895
c_p (kJ/kg K)		1.03939	1.05965	1.1001
μ (Pa s)		1.74684E-5	1.73045E-5	1.73762E-5
k_f (W/m K)		0.0249707	0.0250493	0.0255004

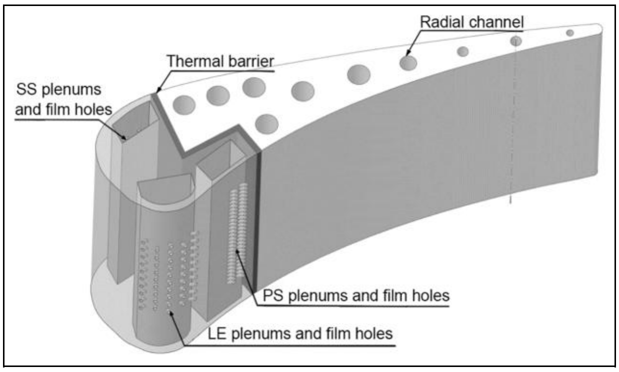

Figure 8. Geometric model of C3X vane.[31]

Table 6. Mainstream conditions of C3X vane.

Parameters	No. 34145
P_0	306,350
T_0	703 K
Inlet *Tu*	6.5%
P_{exit}	212,934 Pa
Ma_{exit}	0.74

Table 7. Coolant conditions at cavity inlet for film cooling of C3X vane.

	Parameters	Pressure side film cooling	Leading edge film cooling	Suction side film cooling
No. 34145	P_0 (Pa)	336,985	321,361	336,066
	T_0 (K)	478.04	513.19	456.95
	$\dot{m}_c$ (g/s)	11.6	7.36	16.9

The boundary conditions applied in the simulation are listed in Table 4, which were derived from the combustion simulation results. Accordingly, the total pressure and temperature were applied at the turbine inlet, whereas the outlet was subjected to a mass flow rate. The rotor speed was set to 13,410.76 RPM. Both adiabatic and isothermal wall simulations were conducted to present the flow characteristics, performance, and the heat transfer characteristics of the gas turbine blade, respectively. For the isothermal simulation, the temperature of the blade wall was 1142 K. In the gas turbine, the working fluid comprises an ideal gas mixture of combustion products (Table 5). The composition of these gases is derived from the results of the combustion simulation (Figure 3). Additionally, we calculated other properties of the working fluid, including heat capacity, dynamic viscosity, and thermal conductivity, using the ideal mixture approach.

Results and discussions

Numerical model validation

NASA's internally film-cooled C3X vane was used to determine the reliability of the suggested process and simulation strategy (Figure 8). Experimental data no. 34145 from Hylton et al.[31] were compared with the simulation results of the C3X model. The main stream and coolant conditions for the C3X model simulations are listed in Tables 6 and 7, respectively.

The surface pressure, temperature, and heat transfer coefficient (HTC) at the midspan of the C3X vane are comparatively presented in Figure 9. As the experimental data ranged from $-25 < X/Ca < 25$, the simulation data were compared with other ranges of the experimental data. As portrayed in Figure 9(a), the pressure values computed from the simulation results using k–ω SST $\gamma - \theta$ turbulence model corresponded well with the experimental data, especially on the pressure side. As depicted in Figure 9(b), the simulation data followed the trend of the experimental data. As observed in Figure 9(c), the HTC in the simulation data were consistent with the experimental data over most of the range, despite the over-prediction of the HTC in the range of $50 < X/Ca < 75$. This phenomenon was caused by the coolant from the suction-side cooling hole. Overall, the maximum deviations in the pressure and temperature were less than 5%, and the mean error

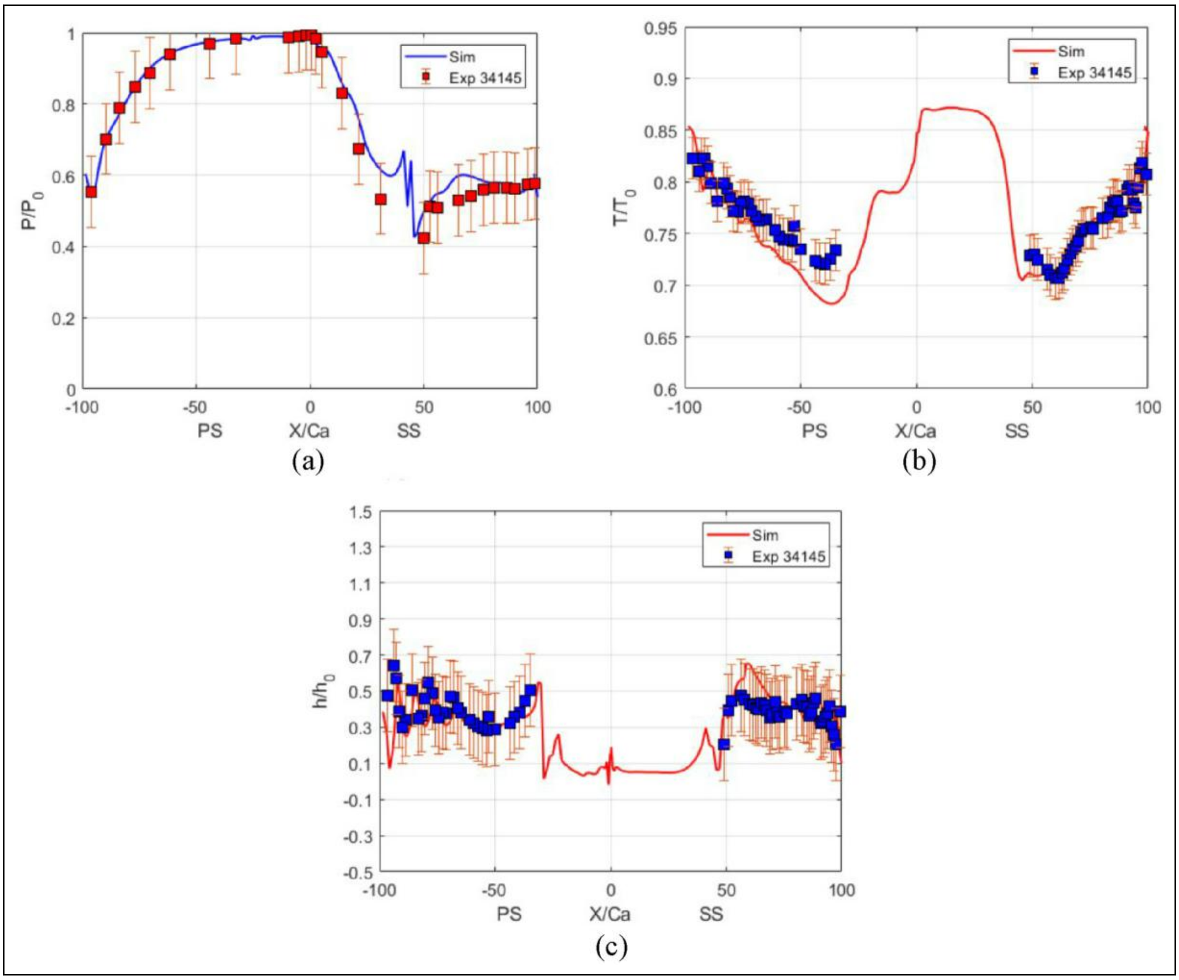

Figure 9. Comparison of predicted (a) pressure, (b) temperature, and (c) HTC on C3X vane surface with those of Case 34,145 from experimental data.

of the HTC calculations was ~22%. Thus, the reliability of the simulation process and strategy was confirmed, similar to a validation reported by Vo.[32,33]

Flow characteristics

The various flow parameters (a) pressure, (b) density, (c) velocity, (d) temperature at the blade midspan are depicted in Figure 10. As confirmed from Figure 10(a), the pressure distribution remained similar throughout the first stage for all types of fuel. However, a pressure reduction was observed in the second stage with H2, specifically near the trailing edge of the S2 and R2 regions. Moreover, in Figure 10(b), the H2 flow at the turbine inlet exhibited a lower density than the JetA and CH4 flows. Unlike other fuels, the combustion products of hydrogen composed of water vapor without any carbon dioxide emissions. The low-density distribution of the flow after the hydrogen combustion was maintained while passing through the gas turbine. The high-pressure gradient and low density in the H2 case created a high-velocity region (Figure 10(c)), especially at the downstream of the stators of each stage. As observed in Figure 10(d), a temperature difference was created in the R2 region, CH_4 exhibited the highest outlet temperature among the fuels, whereas H2 has the lowest temperature. The low-temperature region in the H2 case was caused by the reduction of pressure under a similar specific heat ratio.

The vortex structures of various fuels obtained with a lambda two criterion of $-1.4635 \times 10^7\, s^{-2}$ colored by turbulent kinetic energy are depicted in Figure 11, wherein the H2 case generated smaller vortices on the leading edges of S2 and tip of R2 than other fuels. Overall, the structures in the JetA and CH4 cases were similar. Moreover, we observe a reduction in the turbulent kinetic energy of the H2 case in the same region. Thus, when subjected to identical heat input, pressure, and temperature conditions, hydrogen combustion results in an augmented velocity field and reduced turbulence in the proximity of the blade, as compared to other fuels. These alterations in flow characteristics significantly impact both heat transfer properties and turbine performance, which will be further discussed below.

Heat transfer characteristics

The 2-stage flow parameter distribution including the pressure and temperature on all two-stage blade

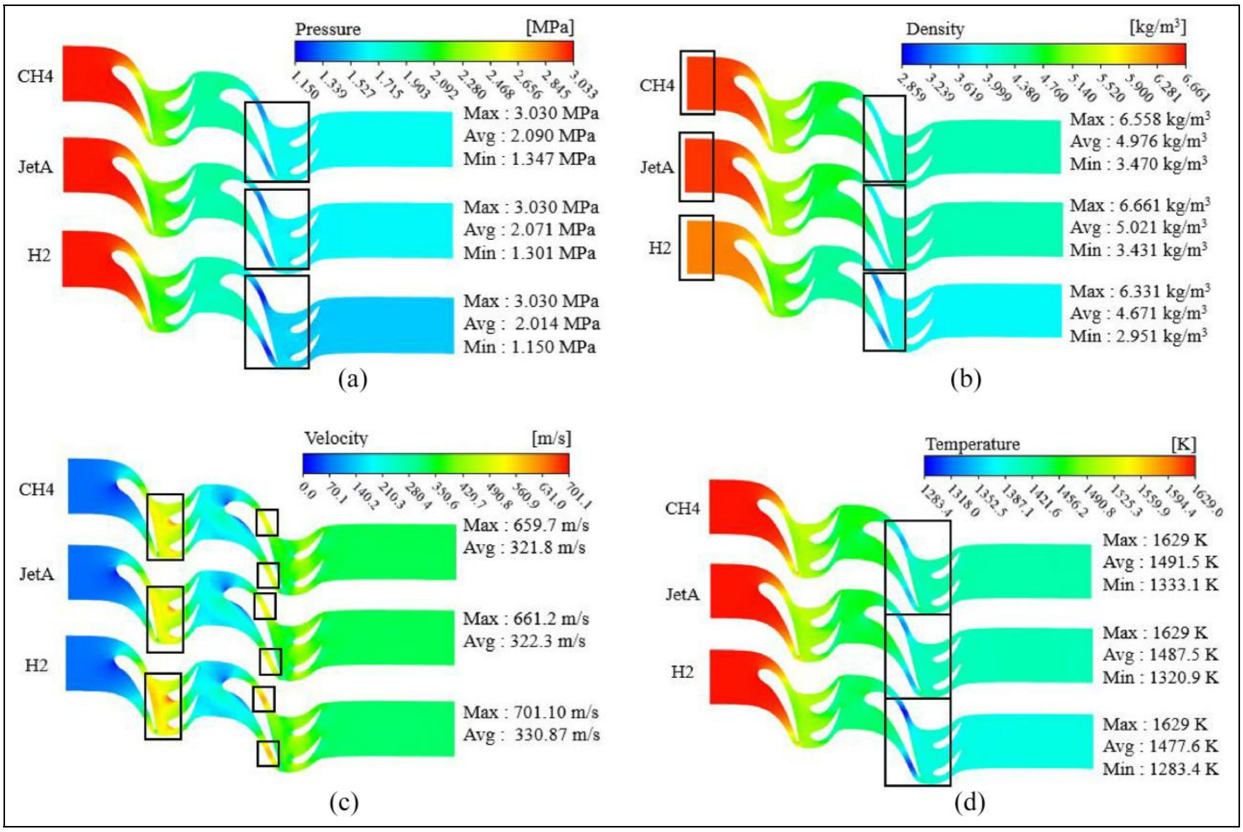

Figure 10. Two-stage flow parameter distribution on blade midspan and maximum, average, minimum values: (a) pressure distribution, (b) density distribution, (c) velocity distribution, and (d) temperature distribution

midspan is illustrated in Figure 12. In Figure 12(a), a pressure reduction was observed in the H2 case in the tip region of the R1 and R2 suction sides, whereas it increased in the CH4 case in the same region. Additionally, the overall pressure distribution was lower for the H2 second-stage blades. In Figure 12(b), a high-temperature region was detected on the suction side near the R1, S2, and R2 tip regions for all the fuel types. In both stages, the JetA and CH4 cases exhibited a high-temperature zone on the tips of the rotors; however, this zone diminished in the H2 case. Under constant heat input rate at the combustor and turbine inlet temperature conditions, the gas turbine blades in the gas turbine section following hydrogen combustion were exposed to a low-temperature flow, which reduced the likelihood of fatigue damage compared to other fuels.

The maximum and area-averaged blade temperatures for each blade are presented in Figure 13, indicating that the maximum temperature of the blade decreased from ~1630 K at S1 to ~1500 K at S2, followed by an increase to ~1540 K for both the JetA and CH4 cases, and a similar temperature at S2 for the H2 case. Although the average temperature of the blades decreased rapidly from S1 to R1, the temperature varied less after the downstream of R1 across all the fuel types. The average temperature at S1 was similar across all fuels at 1613 K, but for H2, the slope of the temperature reduction was greater than that of JetA, implying an average temperature reduction of ~26 K at R2. Conversely, for CH4, the average temperature increased by ~7 K.

The heat flux distributions for all the blades are displayed in Figure 14. The heat flux of the 1st stage (S1, R1) was higher than that of the second stage (S2, R2) for all fuels. In particular, the H2 case exhibited a high heat flux in the leading-edge hub region in R1, which diminished at S2. The area-averaged heat flux at each blade location is plotted in Figure 15. In the first stage, the flow temperature distribution near the blade appears similar across all cases, making the difference in thermal conductivity the dominant factor. Specifically, the combustion product of the H2 case exhibits the highest thermal conductivity, leading to a notably elevated average heat flux in this stage. However, as we progress to the second stage, we observe diverging temperature distributions among the fuels, where the temperature difference takes precedence over the effect of thermal conductivity. In this context, the H2 case displays a lower fluid temperature, resulting in a comparatively reduced heat flux compared to the other cases.

To quantitatively represent the heat transfer characteristics, the average heat transfer coefficient was evaluated using the following equation:

$$HTC = \frac{q''}{T_{i\_w} - T_{a\_w}} \tag{6}$$

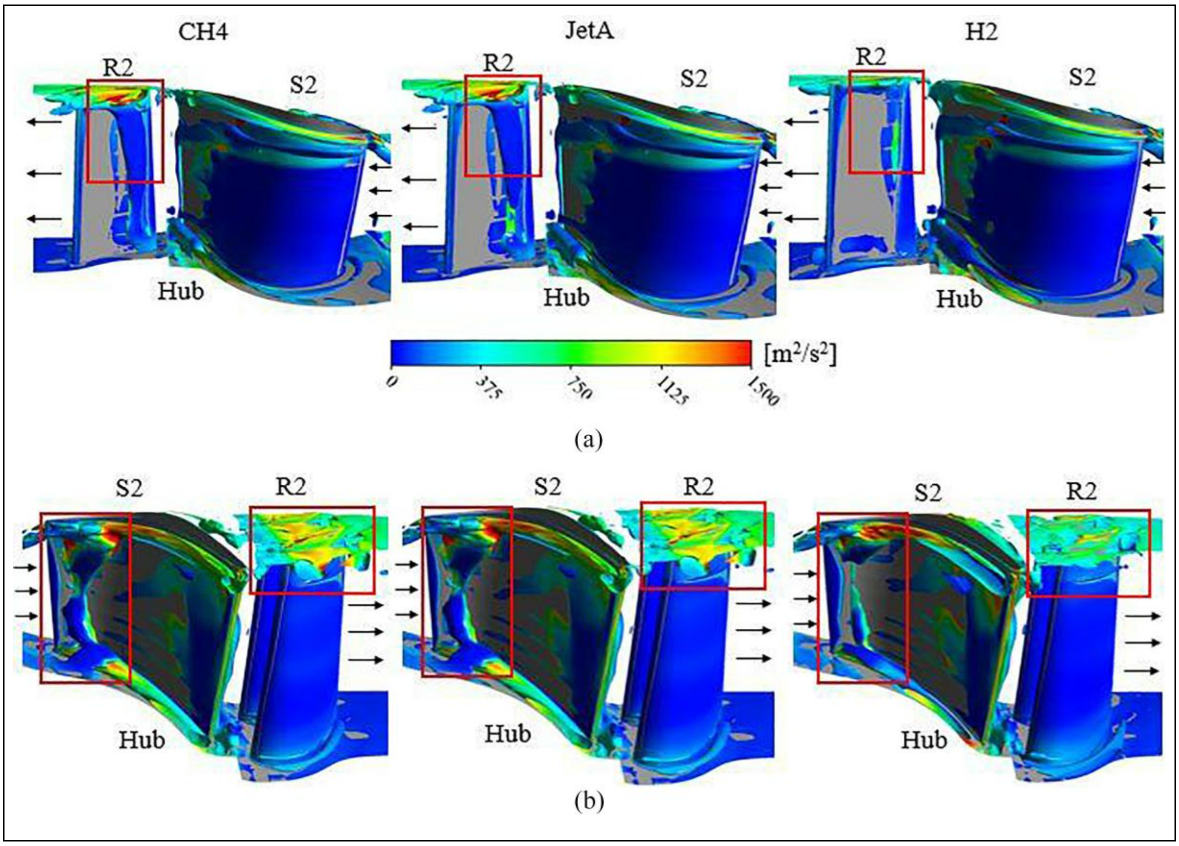

Figure 11. Gas turbine 2nd stage vortex structure of gas turbines for various fuels (Color denotes the turbulence kinetic energy): (a) S2 suction side, R2 pressure side and (b) S2 suction side, R2.

where HTC denotes the heat transfer coefficient, q'' represents the heat flux estimated in the isothermal simulation, T_{i_w} indicates the temperature of the blade surface in the isothermal simulation, and T_{a_w} represents the temperature of the blade in the adiabatic simulation.

The heat transfer coefficient for each blade is depicted in Figure 16, ranging from 2500 to 4200 W/m^{2}K for all blades. For all fuel types, the heat transfer coefficient increased from S1 to R1 and subsequently decreased downstream. Despite exhibiting a high heat transfer coefficient at S1, R1, and S2, the H2 case experienced a reversal at R2 and yielded the lowest heat transfer coefficient. This effect is due to decrease of H2 T_{a_w} on each blade as the flow proceeds to the downstream (Figure 13) and heat flux distribution (Figure 15). In S1, R1, and R2, q'' difference between the fuels is larger than the difference in T_{a_w}. However, in S2, T_{a_w} of H2 case is larger than q'' difference between the fuels. The high heat flux and heat transfer coefficient observed in the first stage signify the requirement of an improved cooling solution in these regions to safely incorporate hydrogen combustion in gas turbines.

Turbine performance

Furthermore, we calculated the power output and thermal efficiency to examine the effects of various fuels on the gas turbine performance. The parameters were evaluated using the following equation:

$$PW_{out} = \tau\omega, \tag{7}$$

$$\eta = \frac{\tau\omega}{\dot{m}_f LHV_f}. \tag{8}$$

In equation (7), PW_{out} denotes the power output of the turbine, τ indicates torque, ω represents angular velocity. In equation (8), η denotes thermal efficiency, $\dot{m}_f$ represents mass flow rate of the fuel, LHV_f indicates the LHV of the fuel. The work of the compressor and additional components was neglected while calculating the thermal efficiency.

The power output and thermal efficiencies of the high-pressure gas turbine for each fuel type are presented in Figure 17, which displayed similar tendencies because of assuming constant heat input for the fuels. The power output and efficiency in the H2 case increased by 25.8% and 30.7% compared to those in the JetA and CH4 cases, respectively.

The cyclic performances were estimated using various fuels in the GE-E^3 engine. The ambient conditions and pressure ratios for each component of the entire GE-E^3 aeroengine are listed in Table 8. Using the isentropic process relation for each component, the total pressure, and temperature can be derived for all the components. The high-pressure spool connects a high-pressure compressor

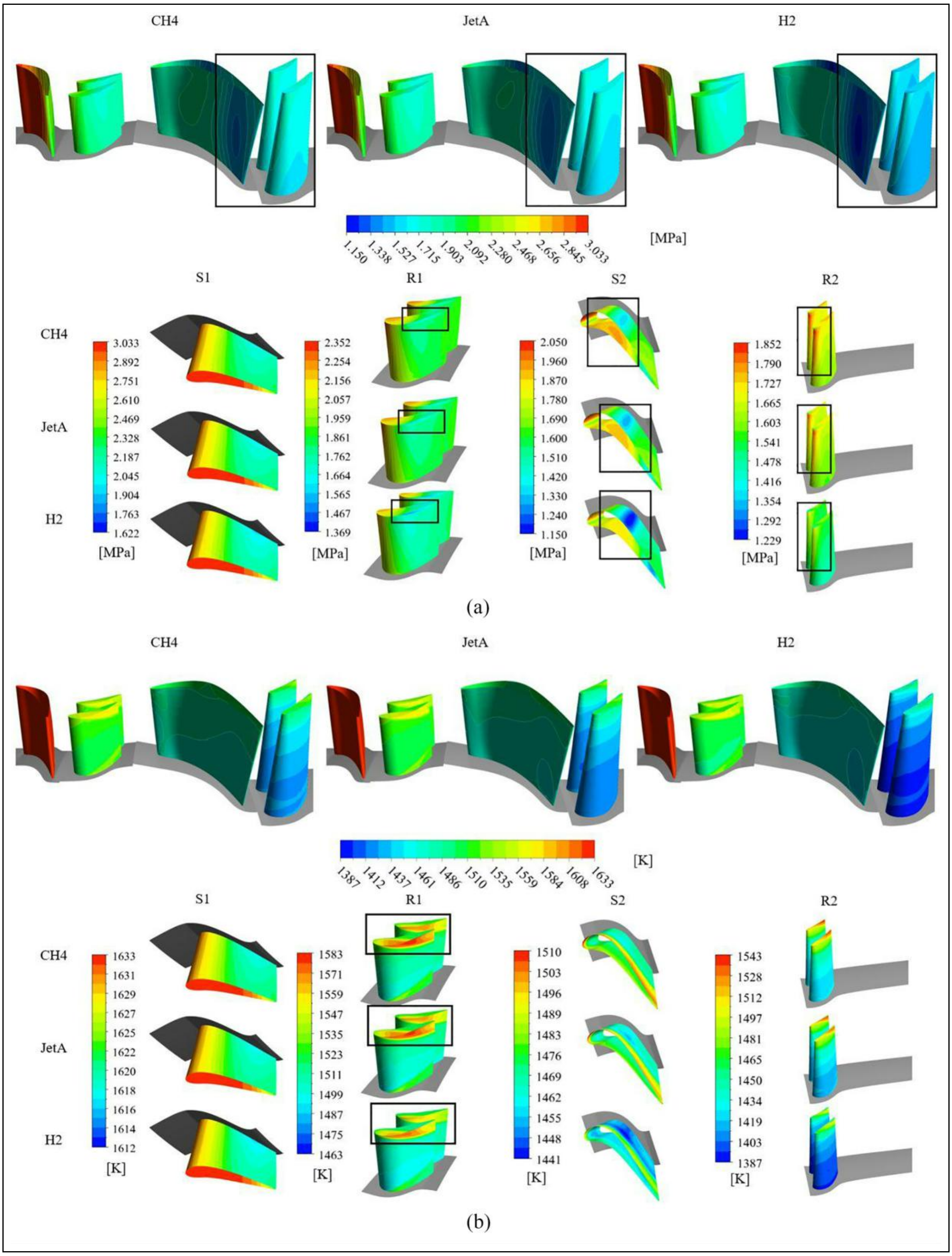

Figure 12. Two-stage flow parameter distribution on blade midspan: (a) pressure distribution and (b) temperature distribution.

(HPT) to a high-pressure turbine (HPT), which is subsequently connected to the fan, low-pressure compressor (LPC), and low-pressure turbine (LPT). Therefore, an equal amount of work was required to connect the spools. Moreover, the critical pressure in the nozzle was evaluated to determine the choked state, and the exit velocity was derived to calculate the thrust of the entire system. The detailed procedure and equations are listed in a previous study.[34]

For each type of fuel, the thrust of the bypass, engine core, and total engine, including the specific thrust of the core and total engine are summarized in Table 9. As observed, the thrust in the core of the system improved the hydrogen combustion system by 3–4% compared to

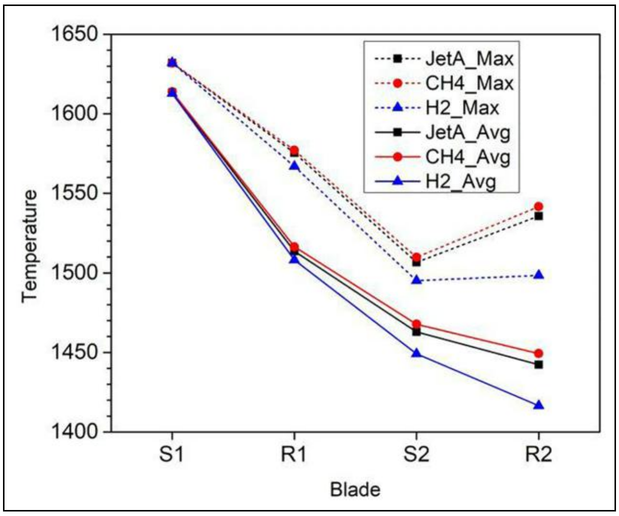

Figure 13. Maximum and area-averaged blade temperatures for each blade.

JetA and CH4, thereby increasing the total thrust by 1.23% and 3.17%, respectively. The specific thrust in the H2 core increased by 3–5%, such that the specific thrust of the engine increased in the H2 case by 1.09% and 3.62% compared to the JetA and CH4 cases.

The engine performance was evaluated using fuel consumption parameters, for example, thrust-specific fuel consumption (TSFC), and brake-specific fuel consumption (BSFC). The TSFC and BSFC of the engine for various fuels are plotted in Figure 18, which exhibited similar trends. The TSFC of H2 was 0.011 kg/s N, corresponding to a reduction of 64.1% and 58.5% compared to that of Jet A and CH4, respectively. Similarly, the BSFC of H2 was 76.1 g/kW h, corresponding to a reduction of 71.4% and 68.1% compared to that of Jet A and CH4, respectively. Overall, the improved fuel consumption per unit of thrust and power in case of using H2 as a fuel confirmed that the current gas turbine system could more efficiently utilize the H2 fuel. Therefore, hydrogen applied gas turbine system can enhance operational efficiency, increasing both operation time, and power output for a given fuel storage capacity. Thus, hydrogen-based operating systems require reduced storage volumes when compared to other fuel alternatives.

Conclusions

In this study, we performed combustion and gas turbine flow simulations to investigate the effect of hydrogen combustion on the GE-E^3 two-stage gas turbine flow, heat transfer characteristics, and performance. Hydrogen combustion was compared with JetA (reference fuel) and CH_4 combustion under constant heat input rate at the combustor, turbine inlet pressure, and temperatures. An equilibrium model based on the HyChem kinetic mechanism was employed to evaluate the combustion product composition of each fuel. Furthermore, the flow characteristics were examined using the k–ω SST γ-turbulence model.

The present results of the hydrogen combustion simulation are summarized as follows:

(1) Under a larger pressure gradient between the stage and low-density flow, the velocity of the H_2 flow increased and its temperature decreased compared with those of JetA and CH_4.

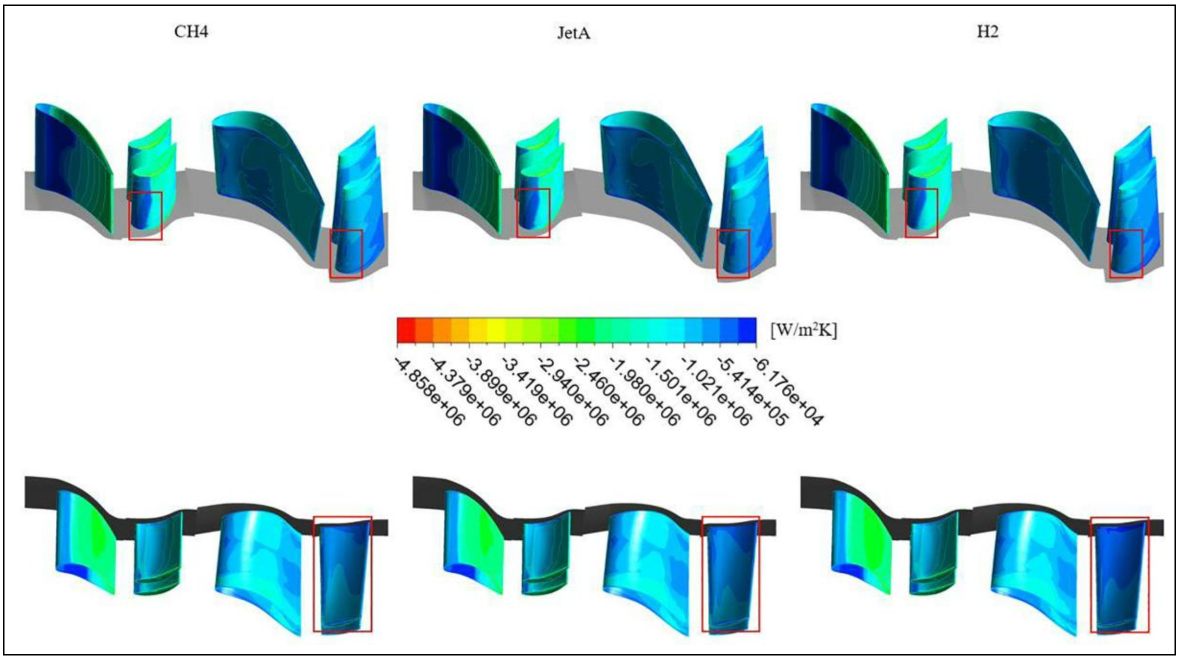

Figure 14. Two-stage blade heat flux distribution.

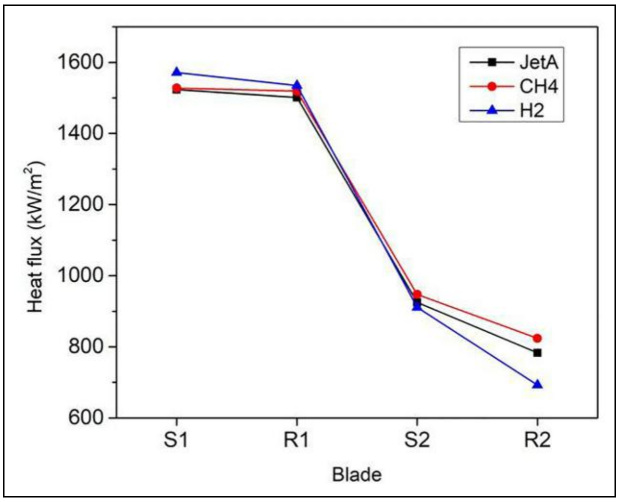

Figure 15. Two-stage blade area-averaged heat flux.

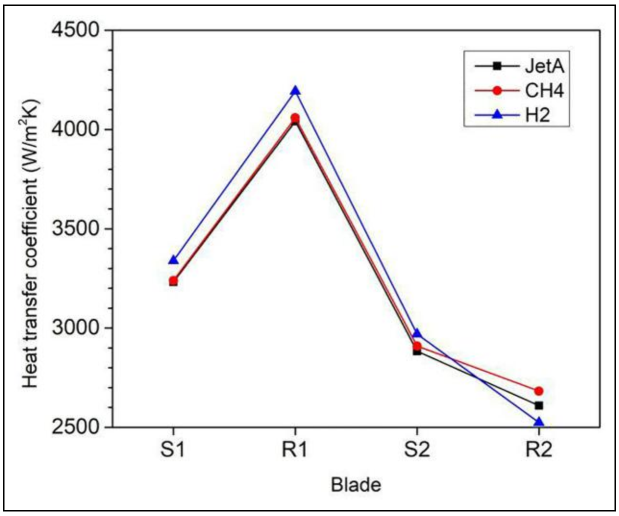

Figure 16. Two-stage blade heat transfer coefficients.

(2) The average heat flux in the H_2 case increased in the first stage, whereas it decreased rapidly in the second stage compared to JetA and CH_4.
(3) The turbine performance improved in H_2 combustion, such that the power output and efficiency increased by 25.8% and 30.7% compared to JetA and CH_4, respectively.
(4) The TSFC and BSFC in the H_2 case improved by 64.5% and 71.4%, respectively, compared with JetA fuel, and by 58.5% and 68.1%, respectively, compared with CH_4.

In conclusion, hydrogen combustion offers not only environmental benefits but also enhances the performance of gas turbine systems. However, the results indicate an increase in heat transfer during the first stage of the gas turbine. Consequently, prior to the development of hydrogen gas turbine systems, it is essential to prioritize the development of an efficient cooling system for the first stage. The findings and simulations presented in this study can provide

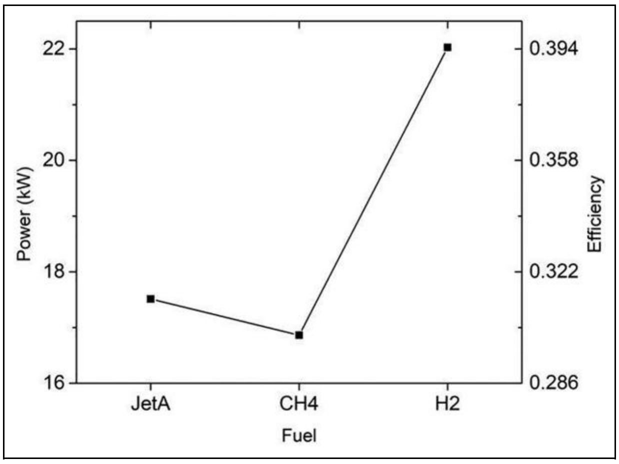

Figure 17. Power output and thermal efficiency of gas turbine.

Table 8. Ambient conditions and pressure ratio at sea level takeoff.

Condition	Value
Altitude	Sea level
Mach number	Static
Ambient temperature	28.9°C
Overall pressure ratio	30.2
Bypass ratio	7.0
Fan outer diameter pressure ratio	1.57
Fan inner diameter & LPC pressure ratio	2.36
HPC Pressure ratio	12.8

Table 9. Thrust, specific thrust, and percentage difference from the reference case. (F_{bypass} denotes the bypass thrust; F_{core} represents the core thrust; F_{total} denotes the total thrust; $F_{core}/\dot{m}_{core}$ indicates the specific thrust of core; $F_{total}/\dot{m}_{total}$ indicates the specific thrust of total engine.).

Parameter	JetA	CH4	H2
F_{bypass} (kN)	109.19	108.02	109.55
F_{core} (kN)	39.58	39.79	41.05
F_{total} (kN)	148.77	147.82	150.60
$F_{core}/\dot{m}_{core}$ (N s/kg)	715.70	729.51	751.21
$F_{total}/\dot{m}_{total}$ (N s/kg)	343.31	334.93	347.07

Reference thrust value: 182.89 kN.

valuable insights for such advancements. Moreover, the study demonstrates the significant influence of external flow from various combustion products on the turbine blade. This, in turn, impacts the structural characteristics of the blade, ultimately affecting its fatigue life. Consequently, future investigations will focus on evaluating the effect of hydrogen combustion in gas turbines through structural analysis and life estimation. These endeavors will help ensure the safe and reliable implementation of hydrogen in gas turbine technology.

Limitation

In an actual combustor, a pressure drop occurs and combustion products from incomplete combustion may

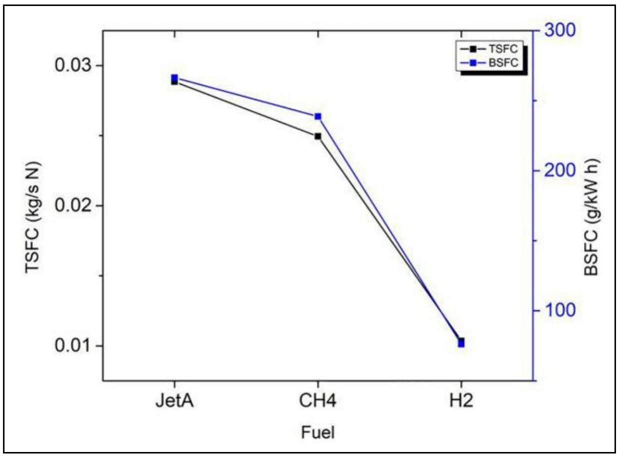

Figure 18. Thrust-specific fuel consumption (TSFC) and brake-specific fuel consumption (BSFC) for various fuels.

be present. In addition, the distribution of the temperature and product concentration profiles differed from the present simulation results. The applied simulation method and the considered assumptions may have affected the flow properties, which induced variations in the result from the actual flow. Moreover, as the cooling structure in the blades was not modeled, the effect of cooling on the turbine was not considered. Despite the limitations regarding the assumptions in the simulation process, this study provided quantitative performance and flow data for various fuels. These data can be used to predict blade fatigue life and aid engineers to design new blade cooling solutions for net zero-emission gas turbines.

Authors' Note

Thanh Dam Mai is also affiliated to Faculty of Mechanical Engineering and Technology, Ho Chi Minh City University of Industry and Trade, Ho Chi Minh City, Vietnam.
Hyeon Kyun Lee is now affiliated to School of Mechanical Engineering, Korea University, Seoul, Republic of Korea.

Author contributions

Conceptualization, methodology, investigation: B. K. and J. R.; formal analysis, writing—original draft preparation, visualization: B. K.; writing—review, and editing: T. D. M., D. T. V., H. K. L. and Y. J.; writing—review and editing, supervision: S. C.; writing—review and editing, supervision, project administration, and funding acquisition: H. L. and J.R. All authors have read and agreed to the published version of the manuscript.

Declaration of conflicting interests

The author(s) declared no potential conflicts of interest with respect to the research, authorship, and/or publication of this article.

Funding

The author(s) disclosed receipt of the following financial support for the research, authorship, and/or publication of this article: This work was supported in part by the Korea Institute of Energy Technology Evaluation and Planning (KETEP) grant funded by the Korean government (MOTIE) (20193310100060, Evaluation of the performance of F-class or more gas turbine blade prototypes). This research was supported by the Korea Electric Power Corporation (Grant number: R21XO01-26).
This research was supported by a Chung-Ang University Graduate Research Scholarship in 2023.

ORCID iDs

Byungwook Kim https://orcid.org/0000-0002-7937-3373
Hyeon Kyun Lee https://orcid.org/0009-0008-5123-6140
Jaiyoung Ryu https://orcid.org/0000-0001-7846-4700

References

1. United Nations. *Energy statistics pocketbook*. *Statistics Papers*. Kenya: United Nations Publications, 2022.
2. Okolie JA, Patra BR, Mukherjee A, Nanda S, Dalai AK and Kozinski JA. Futuristic applications of hydrogen in energy, biorefining, aerospace, pharmaceuticals, and metallurgy. *Int J Hydrogen Energy* 2021; 46: 8885–8905.
3. Frankl S, Gleis S, Karmann S, Prager M and Wachtmeister G. Investigation of ammonia and hydrogen as CO2-free fuels for heavy duty engines using a high pressure dual fuel combustion process. *Int J Engine Res* 2021; 22: 3196–3208.
4. Aasadnia M and Mehrpooya M. Large-scale liquid hydrogen production methods and approaches: a review. *Appl Energy* 2018; 212: 57–83.
5. Nanda S, Vo DVN and Tri PN (eds). *New dimensions in production and utilization of hydrogen*. Elsevier; 2020: 1–20
6. Bohan K, Klapdor EV, Prade B, et al. *Hydrogen power with Siemens gas turbines*. White paper, Siemens Gas and Power GmbH & Co. KG, Germany, 2020.
7. Godmeer J. *Power to gas: hydrogen for power generation*. Report, General Electric Company, 2019.
8. Chiesa P, Lozza G and Mazzocchi L. Using hydrogen as gas turbine fuel. *J Eng Gas Turbine Power* 2005; 127: 73–80.
9. Cappelletti A and Martelli F. Investigation of a pure hydrogen fueled gas turbine burner. *Int J Hydrogen Energy* 2017; 42: 10513–10523.
10. Mai TD and Ryu J. Effects of leading-edge modification in damaged rotor blades on aerodynamic characteristics of high-pressure gas turbine. *Mathematics* 2020; 8: 2191.
11. Mai TD and Ryu J. Effects of damaged rotor blades on the aerodynamic behavior and heat-transfer characteristics of high-pressure gas turbines. *Mathematics* 2021; 9: 627.
12. Nguyen TH, Nguyen-Tri P, Vancassel X and Garnier F. Aero-thermodynamic and chemical process interactions in an axial high-pressure turbine of aircraft engines. *Int J Engine Res* 2019; 20: 653–669.
13. Colket M, Heyne J, Rumizen M, et al. Overview of the national jet fuels combustion program. *AIAA J* 2017; 55: 1087–1104.
14. Xu R, Wang H, Colket M and Edwards T. Thermochemical Properties of Jet Fuels. https://web.stanford.edu/group/haiwanglab/HyChem/approach/ (2015, accessed 28 April 2023).
15. Benaissa S, Adouane B, Ali SM, Rashwan SS and Aouachria Z. Investigation on combustion characteristics and

emissions of biogas/hydrogen blends in gas turbine combustors. *Therm Sci Eng Prog* 2022; 27: 101178.
16. Balli O and Caliskan H. Energy, exergy, environmental and sustainability assessments of jet and hydrogen fueled military turbojet engine. *Int J Hydrogen Energy* 2022; 47: 26728–26745.
17. Reynolds WC. The element potential method for chemical equilibrium analysis: implementation in the interactive program STANJAN. Tech Report.
18. Wang H, Xu R, Wang K, et al. A physics-based approach to modeling real-fuel combustion chemistry – I. Evidence from experiments, and thermodynamic, chemical kinetic, and statistical considerations. *Combust Flame* 2018; 193: 502–519.
19. Xu R, Wang K, Banerjee S, et al. A physics-based approach to modeling real-fuel combustion chemistry – ii. Reaction kinetic models of jet and rocket fuels. *Combust Flame* 2018; 193: 520–537.
20. Burrus D, Chahrour C, Foltz H, et al. *Energy Efficient Engine combustor test hardware detailed design report*. Report, NASA, United States. Report No. NAS 1.26: 168301, 1984.
21. Timko L. *Energy efficient engine high pressure turbine component test performance report*. Report, NASA, United States. Report No. NASA-CR-168289, 1984.
22. Arnone A and Benvenuti E. Three-dimensional Navier-Stokes analysis of a two-stage gas turbine. In: *ASME turbo expo: Power for land, sea, and air*. American Society of Mechanical Engineers; 1994: 78835.
23. Choi MG and Ryu J. Numerical study of the axial gap and hot streak effects on thermal and flow characteristics in two-stage high pressure gas turbine. *Energies* 2018; 11: 2654.
24. Bovo M and Davidson L. Direct comparison of LES and experiment of a single-pulse impinging jet. *Int J Heat Mass Transf* 2015; 88: 102–110.
25. Marocco L. Hybrid LES/DNS of turbulent forced and aided mixed convection to a liquid metal flowing in a vertical concentric annulus. *Int J Heat Mass Transf* 2018; 121: 488–502.
26. Koch J, Schürch C, Wright YM and Boulouchos K. Reactive computational fluid dynamics modelling methane–hydrogen admixtures in internal combustion engines part II: large eddy simulation. *Int J Engine Res* 2021; 22(6): 2054–2068.
27. Ghasemian M, Princevac M, Kim YW and Hamm HD. Numerical modeling of hot gas ingestion into the rotor-stator disk cavities of a subscale 1.5-stage axial gas turbine. *Int J Heat Mass Transf* 2019; 130: 1016–1031.
28. Senel CB, Maral H, Kavurmacioglu LA and Camci C. An aerothermal study of the influence of squealer width and height near a HP turbine blade. *Int J Heat Mass Transf* 2018; 120: 18–32.
29. Galindo J, Serrano JR, García-Cuevas LM and Medina N. Twin-entry turbine losses: an analysis using CFD data. *Int J Engine Res* 2022; 23(7): 1180–1200.
30. Hylton L, Mihelc M, Turner E, et al. *Analytical and experimental evaluation of the heat transfer distribution over the surfaces of turbine vanes*. Report, NASA, United States. Report No. NAS 1.26: 168015, 1983.
31. Hylton L, Nirmalan V, Sultanian B, et al. *The effects of leading edge and downstream film cooling on turbine vane heat transfer*. Report, NASA, United States. Report No. ALLISON-EDR-13481), 1988.
32. Vo DT, Mai TD, Kim B and Ryu J. Numerical study on the influence of coolant temperature, pressure, and thermal barrier coating thickness on heat transfer in high-pressure blades. *Int J Heat Mass Transf* 2022; 189: 122715.
33. Vo DT, Mai TD, Kim B, Jung JS and Ryu J. Numerical investigation of crack initiation in high-pressure gas turbine blade subjected to thermal-fluid-mechanical low-cycle fatigue. *Int J Heat Mass Transf* 2023; 202: 123748.
34. Rogers GFC, Saravanamuttoo HIH, Cohen H and Straznicky P. *Gas turbine theory*. 7th ed. Pearson, 2017.

Appendix

Notation

1–8	Station number
$\dot{m}_f$	Fuel mass flow rate (kg/s)
$\dot{m}_a$	Air mass flow rate (kg/s)
LHV_f	Lower heat value of fuel (MJ/kg)
$\dot{Q}$	Heat input rate (W)
Φ	Equivalence ratio
$\left(\frac{\dot{m}_a}{\dot{m}_f}\right)_{stoic}$	Theorical air–fuel ratio of fuel
$\dot{m}_{total}$	Mass flow rate of air–fuel mixture (kg/s)
y +	Normalized distance from the solid wall
ρ	Density (kg/m^3)
u	Velocity (m/s)
P	Pressure (Pa)
μ	Dynamic viscosity (Pa·s)
E	Specific internal energy (J)
μ_{eff}	Effective dynamic viscosity (Pa·s)
k_{eff}	Effective thermal conductivity (W/m·K)
c_p	Specific heat on constant pressure (kJ/kg·K)
k_f	Fluid thermal conductivity (W/m·K)
X	Axial distance (m)
Ca	Axial chord length (m)
P_0	Total pressure (Pa)
T_0	Total temperature (K)
Tu	Turbulence intensity
P_{exit}	Exit pressure (Pa)
Ma_{exit}	Exit mach number
$\dot{m}_c$	Coolant mass flow rate (g/s)
HTC	Average heat transfer coefficient (W/m^2·K)
q''	Heat flux (W/m^2)
T_{i_w}	Temperature of blade in isothermal simulation (K)
T_{a_w}	Temperature of blade in adiabatic simulation (K)
PW_{out}	Power output (kW)
τ	Torque (N·m)
ω	Angular velocity (rad/s)
η	Total-to-total efficiency
F_{bypass}	Bypass thrust (kN)
F_{core}	Core thrust (kN)
F_{total}	Total thrust (kN)
$F_{core}/\dot{m}_{core}$	Specific thrust of core
$F_{total}/\dot{m}_{total}$ (N s/kg)	Specific thrust of total engine